

---

# A FINITE DIFFERENCE THERMAL MODEL OF A CYLINDRICAL MICROWAVE HEATING APPLICATOR USING LOCALLY CONFORMAL OVERLAPPING GRIDS: PART II - NUMERICAL RESULTS AND EXPERIMENTAL EVALUATION

---

Hussain M. Al-Rizzo<sup>1</sup>, Rami Adada<sup>1</sup>, Jim M. Tranquilla<sup>2</sup>,  
Feng Ma<sup>2</sup> and Bogdan C. Ionescu<sup>3</sup>

<sup>1</sup>Systems Engineering Department, Donaghey College of Information Science and Systems  
Engineering, University of Arkansas at Little Rock, USA

<sup>2</sup>Electrical and Computer Engineering Department, University of New Brunswick, Canada

<sup>3</sup>Ansoft Corporation, [www.ansoft.com](http://www.ansoft.com)

*In this paper, we present numerical results obtained from a robust, locally conformal 3-D Orthogonal Grid Finite Difference (OGFD) thermal algorithm introduced in Part I of our current investigation [Al-Rizzo et al., 2006] integrated with an Orthogonal Grid Finite-Difference Time Domain (OGFDTD) scheme [Al-Rizzo et al., 2000], which accurately models the volumetric electromagnetic (EM) power deposition pattern. A unified meshing scheme, which utilizes identical overlapping grids in Cartesian and cylindrical coordinates, is employed within the load zone in the OGFDTD and OGFD models. Local temperature profiles excited by the absorbed microwave energy were measured at seven locations within the sample as a function of heating time. In order to benchmark, or validate our model, an alternative analysis of the coupled EM and thermal simulations was performed using state-of-the-art, Finite Element Method-based Ansoft's High Frequency Structure Simulator (HFSS) and the coupled thermal/stress analysis tool ePHYSICS (<http://www.ansoft.com>). Additionally, we compare our numerical simulations against measured dynamic temperature profiles induced within a mineral ore sample maintained for exposure period of 28.5 minutes inside a cylindrical multimode heating furnace energized at 915 MHz with a microwave source power of 12.5 kW and accompanied with significant temperature elevation. A combination of convective and radiation thermal boundary conditions are considered at the interfaces between the cavity walls, air, and sample. There is a general agreement between simulated and measured spatial and temporal temperature profiles, which validates the proposed model. Results indicate that inevitable fluctuations in the frequency spectrum and output power of the magnetron, non-uniformity of sample packing, and heat released by uncontrolled exothermic chemical reactions have a significant effect on the comparisons between measured and computed temperature patterns.*

---

**Keywords:** Cavity Resonator, Finite Difference Method, Locally Conformal Overlapping Grids, Microwave Heating, Thermal Modeling

**Submission Date:** February 17, 2005

**Acceptance Date:** July 21, 2006

---

## INTRODUCTION

Interest in applying microwave heating to material processing has been intensively pursued over the last several decades [Al-Rizzo *et al.*, 2000; Filfet *et al.*, 1996; Iskander *et al.*, 1994; Material Research Society, 1996]. High-power microwave processing of materials, which has enormous potential in a diversity of industrial applications, possesses several compelling advantages due to its energy efficiency, selectivity, and volumetric heating nature.

The majority of industrial applications employ a multimode cavity furnace in which numerous standing-wave resonant modes exist simultaneously in a given frequency range [Al-Rizzo *et al.*, 2000; Braunstein *et al.*, 1999; Clemens *et al.*, 2000; Dibben, 1995; Iskander *et al.*, 1994; Ma *et al.*, 1995; Torres and Jecko, 1997; Tranquilla *et al.*, 1999]. A multimode cavity is a versatile applicator in that it can be adapted to a wide range of materials of different dielectric properties, sizes, and shapes. However, it suffers from two major drawbacks: the EM field distribution is not well defined and the power density is relatively small within the sample volume [Materials Research Society, 1996].

Although microwave heating has been extensively utilized so far in domestic and industrial applications, the design of a specific applicator system at present is usually an empirical process relying on accumulated experience, analytical solutions to idealized cases, and trial-and-error experimental procedures. Reliable and repeatable experimental design methods are rather expensive and time consuming due to the several interacting physical mechanisms involved.

The task of modeling a microwave heating process is by no means a simple endeavor. Microwave heating processes are notoriously complex and generally cannot be solved analytically. The existence of a simulation tool capable of characterizing a realistic microwave

heating process would reveal a valuable insight into the factors that influence the dynamics of temperature diffusion. To this end, the prospects of modeling a microwave heating process may aid system engineers posed with challenges to provide innovative solutions to characterize the basic nature of the physical phenomena involved, identify critical parameters to enhance energy coupling into the workload, and provide a rapid design of optimized and controllable systems.

Remarkable progress has been achieved in recent years in research and development utilizing computer simulations where numerous problems, which previously were intractable, have been solved with several valuable results being reported [Al-Rizzo *et al.*, 2000; Braunstein *et al.*, 1999; Clemens *et al.*, 2000; Dibben, 1995; Filfet *et al.*, 1996; Gamos, 1998; Haala and Wiesbeck, 2002; Iskander *et al.*, 1994; Ma *et al.*, 1995; Torres and Jecko, 1997; Tranquilla *et al.*, 1999]. Due to the relatively low cost, time saving, and repeatability, computer simulations can often complement and reduce the empiricism involved in an otherwise purely experimental approach; particularly, in initial design and prototyping studies allowing microwave applicators to be characterized carefully prior to high power testing.

While the Finite-Difference Time Domain (FDTD) technique continues to enjoy an ever-increasing popularity due to its simplicity, efficiency, and generality, there have been very few publications that address the problem of cylindrical multimode cavity resonators. This problem has proved a difficult challenge, which has not yet been satisfactorily resolved [Dibben, 1995; Gamos, 1998; Al-Rizzo *et al.*, 2000]. Due to space limitations, we do not provide a comprehensive review of the literature in regard to the application of the FDTD to the analysis and design of microwave ovens. However, as far as multimode cavity resonators are concerned, a close scrutiny of the literature revealed that, with a few exceptions, previously published FDTD, finite element, and method of moment's

---

models have all been restricted to or designed specifically to isolated regular rectangular geometries [Materials Research Society, 1996]. This approach neglects interactions due to the exchange of energy with the external source. Another simplifying assumption commonly invoked is that the cavity walls are replaced by Perfectly Electric Conducting (PEC) surfaces when the EM continuity conditions are imposed. Furthermore, the majority of recent measurement and modeling studies have been carried out on laboratory-scale applications. Moreover, there is very little information available on aperture-coupled cylindrical multimode applicators, which may provide increased spectral density and, in certain circumstances, yield better performance than rectangular geometries of the same volume [Tranquilla *et al.*, 1999; Al-Rizzo *et al.*, 2000].

We have developed a 3-D locally conformal Orthogonal Grid Finite-Difference Time Domain (OGFDTD) scheme which implements Cartesian and cylindrical overlapping grids for the simulation of dissipated EM power, resonant frequencies, and return loss of a pilot scale, partially loaded cylindrical multimode microwave furnace of a large throughput with a concentric rectangular aperture in the transverse plane [Tranquilla *et al.*, 1999]. The salient feature of the model is that power losses due to the finitely conducting coupling waveguide and cavity walls are incorporated using the concept of surface impedance boundary conditions [Al-Rizzo *et al.*, 2000]. We focus our attention in this paper on solving the Coupled Electromagnetic-Thermal (CET) problem where the temperature dependency of the constitutive parameters is a key element in the analysis. In the first part of this study [Al-Rizzo *et al.*, 2006]; we formulated a new explicit Orthogonal Grid Finite-Difference (OGFD) thermal model to allow comprehensive simulations of dynamic temperature profiles. The OGFD model is based on the same gridding scheme of the OGFDTD in the sample zone while taking into account the non-uniformity

of cell dimensions at the interfaces between the processed material and applicator walls. Significant heat loss mechanisms, including convection/radiation at the interface between the workload and air inside the cavity, heat convection/radiation between the exterior and interior surfaces of the cavity and the surrounding media, are taken into consideration. It should be remarked that the model, however, ignores material phase-transition, heat release by exothermic chemical reactions as well as any presence of liquids or vapor within the material to be processed.

It must be pointed out that as far as microwave heating in multimode cavities is concerned, earlier and most recent work were confined to domestic-sized ovens within relatively short heating durations ranging from several seconds up to a few minutes with the accompanying rise in temperature being below 300 °C [Ma *et al.*, 1995; Torres and Jecko, 1997; Dibben, 1995]. In this second part, we report modeling and numerical analysis together with experimental data to scale up existing models to production-scale industrial applicators with a view to optimize performance and to predict the heating profiles over sufficiently prolonged microwave heating exposure periods during which the power deposition and temperature may change substantially due to thermodynamic processes.

The frequency spectrum of commercial magnetrons drastically fluctuates during processing due to changes in the load impedance. We have investigated the consequences on a lightly loaded resonant applicator, whereby small fluctuations in the center frequency of the magnetron and/or output power can produce large changes in the instantaneous dissipated EM power and, hence, significant changes in the predicted temperature profiles.

The model is benchmarked against a physical heating experiment carried out using an aperture-coupled cylindrical multimode applicator with 12.5 kW incident microwave power at 915

MHz. The holding time used in the experiment was 28.5 minutes with temperature rise in hot spots being well above 400 °C using a mineral ore sample with known dielectric properties versus temperature. Numerical simulations from the present approach are found to be in a good agreement with those derived from HFSS and ePHYSICS which proved the validity of the OGF D scheme. Results obtained from the OGF D model show a reasonable agreement with the experimental data and consistently predicted the observed trends of the heating patterns evolved inside the workload.

## EXPERIMENTAL RESULTS

The microwave heating applicator under consideration is a partially filled cylindrical multimode cavity connected to a WR-975 rectangular waveguide, which is fed by a 75 kW (maximum), 915 MHz magnetron. Based on our CET model, the dimensions of the applicator and coupling aperture were selected to provide sufficiently overlapping modes to maintain a prescribed heating profile within the frequency spectrum of the magnetron, coupled with the size and nature of the load. The applicator, associated circuitry and control have been designed,

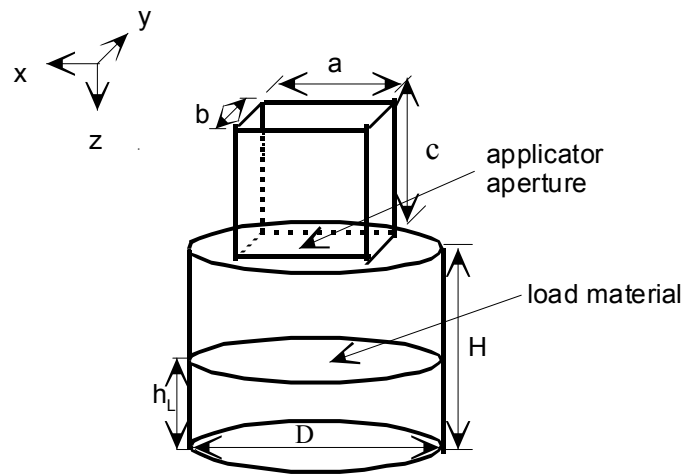


**Figure 1.** Geometry of the aperture-coupled multimode cavity applicator

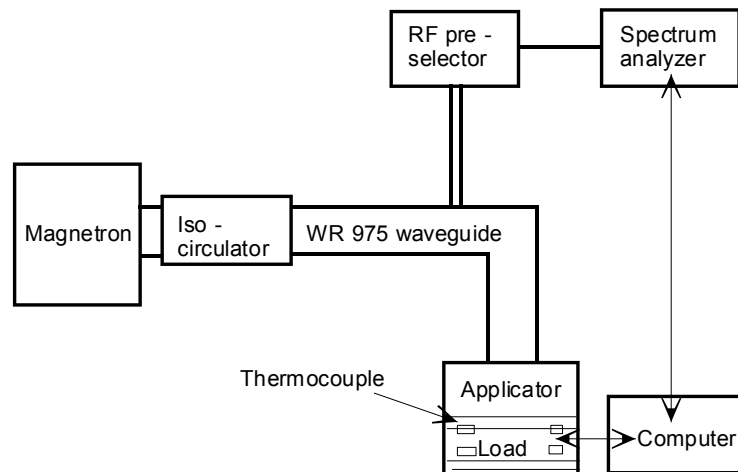


**Figure 2.** A schematic diagram of the experimental setup used in the microwave heating experiment

---

tested, and integrated into a pilot plant with the objective of developing unique microwave heating processes for the pretreatment of mineral ores and concentrates.

Figure 1 depicts the microwave heating applicator, which is a section of a circular cylindrical cavity of diameter  $D = 30.48$  cm and height  $H = 116.84$  cm with a concentric rectangular aperture in the transverse plane. The applicator is constructed from stainless steel with a lateral wall thickness,  $w_s = 0.95$  cm; top and bottom wall thickness,  $w = 0.95$  cm. The cavity is loaded with a mineral ore sample of height  $h_L = 22.9$  cm.

A schematic diagram of the experimental setup is shown in Fig. 2. A spectrum analyzer is used to monitor the forward power delivered by the magnetron and power reflected from the cavity. Inside the applicator, seven thermocouples are placed in two layers to monitor the temperature, which is recorded by a data acquisition computer. One layer, with four thermocouples, is positioned parallel to and 12.7 cm above the bottom of the applicator. This layer is called the “Bed Middle” layer. The other layer, which contains three thermocouples, called the “Bed Top” layer, is located on a plane parallel to and 20.3 cm above the bottom of the applicator. In the “Bed Middle” layer, the four thermocouples are set at  $\phi = 45^\circ$  ( $\phi = 0^\circ$  refers to the  $x$  axis in Fig. 1),  $-45^\circ$ ,  $135^\circ$ , and  $-135^\circ$ . For the “Bed Top” layer, the three thermocouples are set at  $\phi = 135^\circ$ ,  $-135^\circ$ , and  $-45^\circ$ . All the seven thermocouples, which are built within the cavity, are placed 0.95 cm away from the interior surface of the sidewall and are immersed within the load material.

It is well known that metallic thermocouples exposed to intense microwave fields will not read correctly due to microwave heating. To calibrate the temperature acquisition system, several tests were conducted to compensate for this effect whereby the microwave power source was cycled on and off to record any jumps in the readings of the thermocouple sensors. It should

be noted that the sensors were installed deep to the surface where the microwave power density is small.

The generator is set at a nominal output power of 12.5 kW. The curing process lasted for 28.5 minutes. One key step of the experiment is loading the material. A very fine, sand-like ore material, with a particle size distribution in the range of 100 - 150  $\mu\text{m}$ , was loaded. To minimize air pockets, the sample was compacted, including around the thermocouples.

Figures 3 and 4 exhibit the temperature evolutions measured by the thermocouples on the “Bed Middle” and “Bed Top” layers. Theoretically, the four thermocouples on the “Bed Middle” should have yielded identical temperatures due to the axial symmetry of the system and EM fields. This should also be the case for the three thermocouples on the “Bed Top”. Actually, discrepancies were observed among the temperatures measured by the four thermocouples of “Bed Middle” and among the temperatures measured by the three thermocouples of “Bed Top.” These discrepancies are attributed to the unavoidable non-uniformity of material loading and level of compaction, which resulted in an inhomogeneous and unpredictable spatial distribution of material parameters.

## NUMERICAL RESULTS AND COMPARISON WITH MEASUREMENTS

In this section, our CET model is used to simulate the microwave heating process, and the results are compared against those obtained from Ansoft’s ePHYSICS as well as experimental data. A selection of these results is provided including power and temperature measurements.

Knowledge of the dielectric and thermo-physical properties of the processed material is imperative to achieve realistic simulations of heat transfer processes. Though we are certain that a comprehensive set of measurements is not

**Figure 3.** Temperature profiles measured by the thermocouples on the “Bed Middle” layer

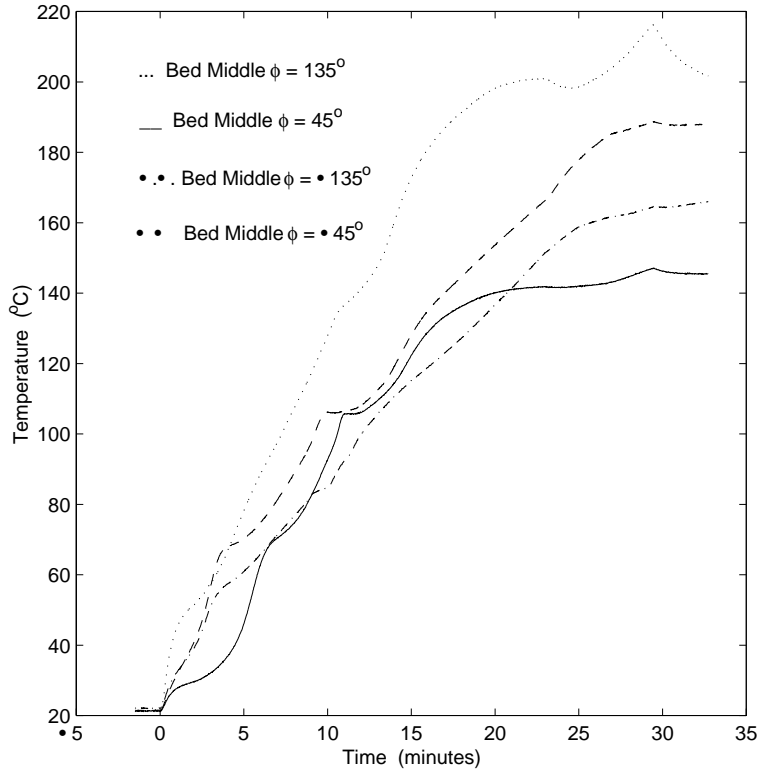
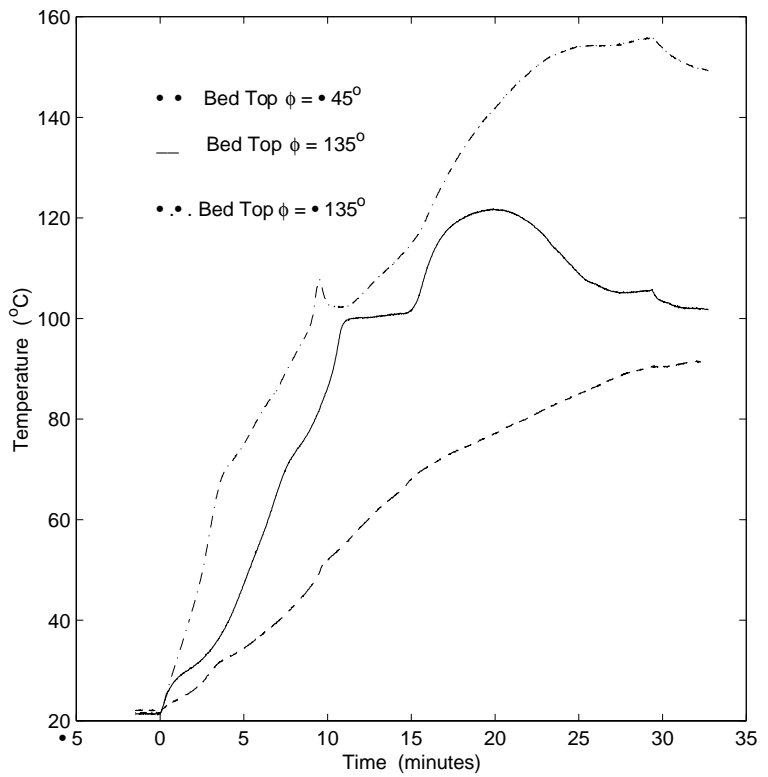


**Figure 4.** Temperature profiles measured by the thermocouples on the “Bed Top” layer



currently available, we made use of the most complete and reliable compilation of published data. In the absence of reliable measured data, the thermo-physical properties of the work piece are considered to be temperature independent. The complex relative dielectric constant of the processed material,  $\epsilon_r = \epsilon_r' - j \epsilon_r''$  was measured at a frequency of 912 MHz as a function of temperature over the range from 22 ° C to 688 ° C. The availability of the permittivity as a function of temperature allows the EM fields to be updated versus temperature change leading to better simulation accuracy.

The specific heat capacity, thermal conductivity, and density of stainless steel are respectively taken as  $c_{pw} = 468$  J/kg.K,  $k_w = 13.4$  W/m.K, and  $\rho_w = 8238$  kg/m<sup>3</sup>; the corresponding values for the processed material are considered to be temperature independent and respectively taken as  $c_{pd} = 980$  J/kg.K,  $k_d = 0.265$  W/m.K, and  $\rho_d = 2200$  kg/m<sup>3</sup>. The value of  $k_d$  is based upon the constituents of the material and  $\rho_d$  is calculated by the vessel's volume and the amount of material used in the experiment. The specific heat capacity and density of air are taken as  $c_{p\_air} = 1009.0$  J/kg.K, and  $\rho_{air} = 0.998$  kg/m<sup>3</sup>.

The convection heat transfer coefficients  $h_2, h_4, h_5, h'_5, h_6,$  and  $h'_6$  introduced in [Al-Rizzo *et al.*, 2006] are determined as follows:

$$h_2 = 6.1 \left( \frac{T_i}{T_{air\_out}} - 1 \right)^{0.25} \quad (1)$$

$$h_4 = 6.1 \left| \frac{T_i}{T_{air\_in}} - 1 \right|^{0.25} \quad (2)$$

$$h_5 = 10.8 \left( \frac{T_i}{T_{air\_out}} - 1 \right)^{0.25} \quad (3)$$

$$h_6 = \begin{cases} 5.5 \left( \frac{T_i}{T_{air\_in}} - 1 \right)^{0.25}, & T_i \geq T_{air\_in} \\ 11.0 \left( 1 - \frac{T_i}{T_{air\_in}} \right)^{0.25}, & T_i < T_{air\_in} \end{cases} \quad (4)$$

$$h'_5 = \begin{cases} 11.0 \left( \frac{T_i}{T_{air\_in}} - 1 \right)^{0.25}, & T_i \geq T_{air\_in} \\ 5.5 \left( 1 - \frac{T_i}{T_{air\_in}} \right)^{0.25}, & T_i < T_{air\_in} \end{cases} \quad (5)$$

$$h'_6 = 5.4 \left( \frac{T_i}{T_{air\_out}} - 1 \right)^{0.25} \quad (6)$$

where  $T_i$  is the temperature at the material-air interface,  $T_{air\_in}$  is the time-dependent temperature of air inside the cavity, and  $T_{air\_out}$  is the temperature of air outside the cavity. Since the side walls of the applicator were thermally insulated, then  $h_2 = 0$ .

Accurate simulation of a realistic microwave heating experiment requires careful consideration of the power spectrum of the generator. The magnetron used has a nominal center frequency of 915 MHz with a bandwidth of 50 MHz. However, the spectrum may shift during operation, especially at lower power levels. Figure 5 shows the power spectrum of the forward and reflected signals measured at different instants during the experiment. It can be seen that the center frequency of the magnetron was around 909 MHz with a 3-dB bandwidth of 1.2 MHz.

To gain an insight into the coupling efficiency of the loaded cavity in the desired frequency range around the nominal center frequency, Fig. 6 displays the spectrum of  $S_{11}$  within the operating frequency range of the magnetron calculated using our OGFDTD model under the same experimental loading conditions using  $\epsilon_r = 4.2 - j0.25$ , which is representative for the permittivity of the processed material. The reflected power spectrum (shown in Figs. 5 (b), (c), and (d)) can be approximately seen as the sum of the forward power spectrum (shown in Fig.5 (a)) and the reflection coefficient shown in Fig. 6 (noting that in Figs. 5 and 6 the units are in dBm and dB, respectively). The reflection coefficient displayed in Fig. 6 is not flat in the frequency band of interest, 890-920 MHz;

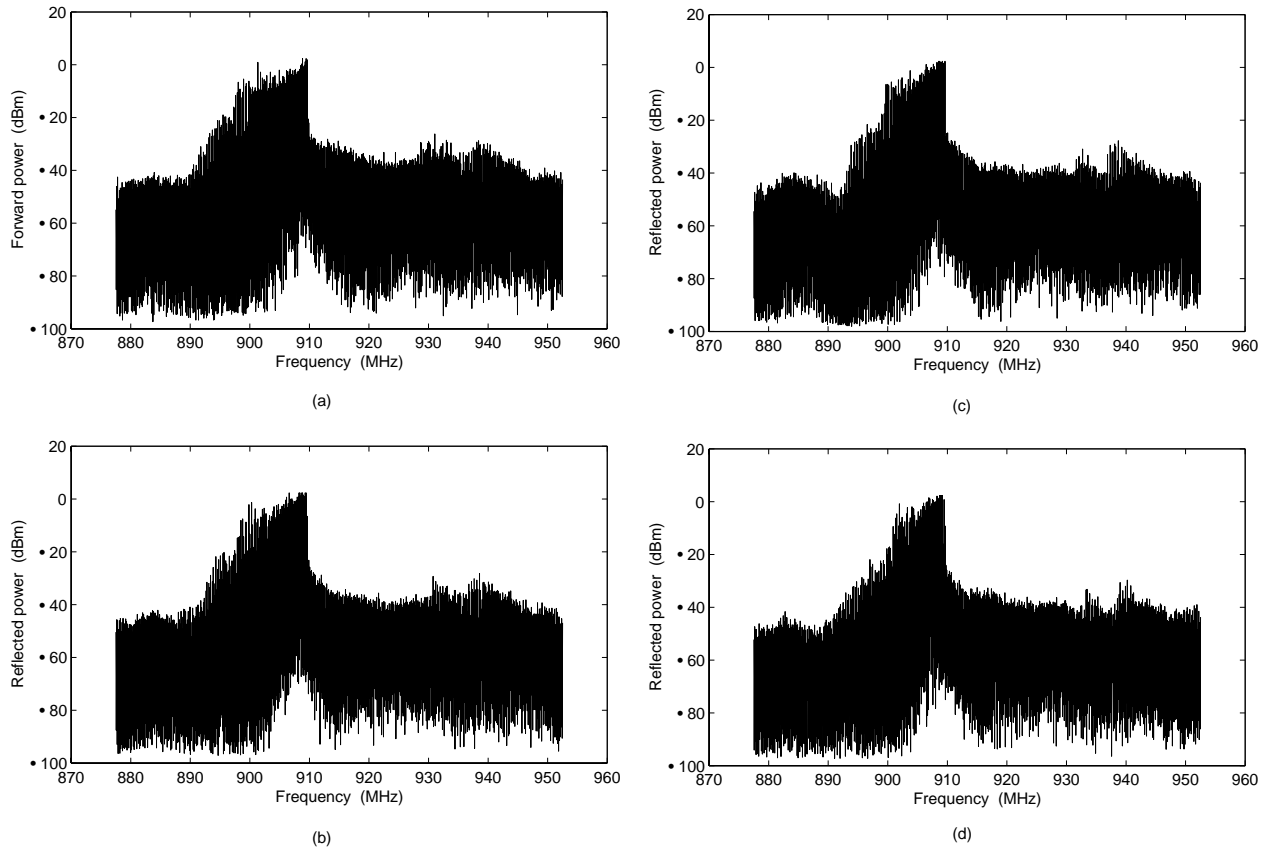
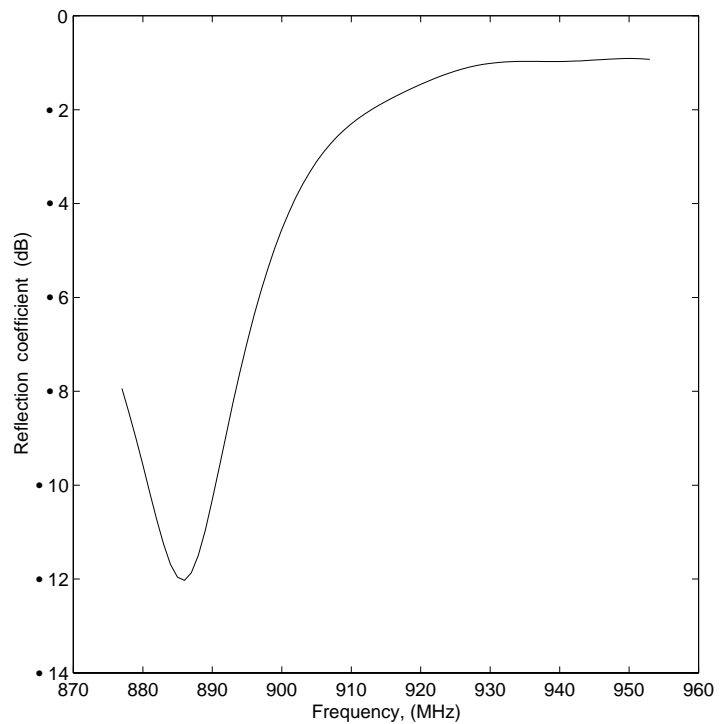


**Figure 5.** Measured power spectrum: (a) forward power spectrum after 232 seconds, (b) reflected power spectrum after 232 seconds, (c) reflected power spectrum after 720 seconds, and (d) reflected power spectrum after 1287 seconds

**Figure 6.**  $S_{11}$  spectrum of the loaded cavity calculated for  $\epsilon_r = 4.2 - j0.25$



therefore, selecting different frequencies in the model will definitely affect the coupling of the microwave energy and hence the prediction of the induced temperature profile. A center frequency of 909 MHz is chosen to run the CET model, and the results were compared against those calculated at 915 MHz.

The interior surfaces of the cavity have been polished. Even so, reflections impinge on other surfaces of the workload. We were dealing with a multiple body heat transfer problem whereby the calculation of the combined configuration-emissivity factor,  $f_{ce}$  [Al-Rizzo *et al.*, 2006] is not a trivial task. This factor depends on the geometry of the cavity, load material, and surface temperature. A generalized linear boundary, described in [Al-Rizzo *et al.*, 2006] with an equivalent heat transfer coefficient is employed in our CET scheme to model heat convection and radiation.

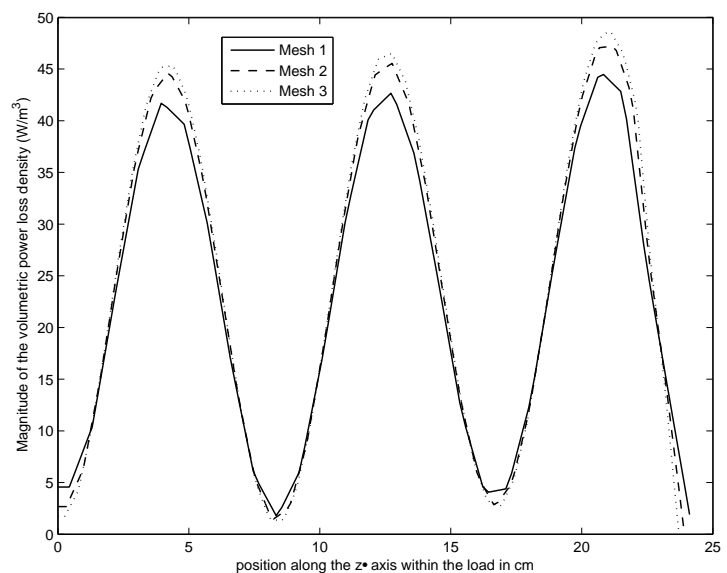
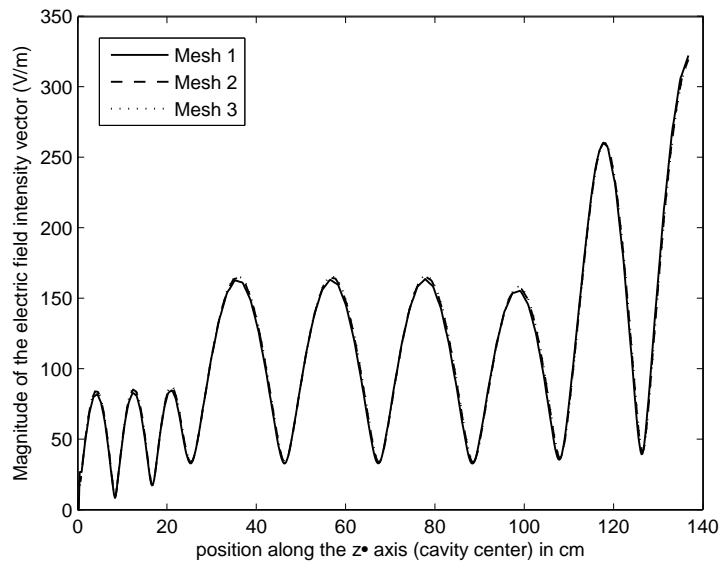
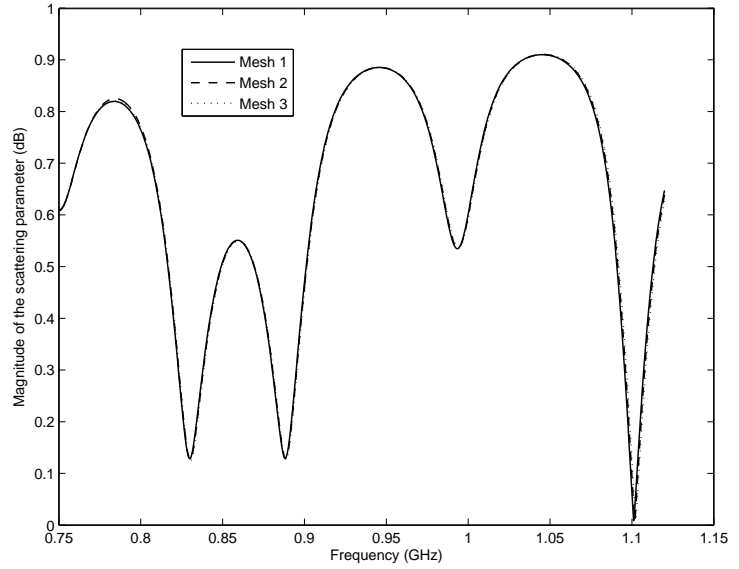
Several systematic testing procedures were implemented in order to check the validity of the proposed CET scheme and to verify the accuracy of computations. In all cases to be presented, a convergence test has been carried out to ensure that the EM fields and temperature have been sufficiently sampled in space by varying the number of grid points in an iterative process to determine the mesh resolution required for a predetermined convergence criterion. Convergence is determined in the Cauchy sense, i.e., accuracy is based on the criterion of the relative constancy of EM and thermal parameters when at least two consecutive meshing structures result in a specified percentage difference. Convergence of the EM results is indicated from the frequency spectrum of the scattering parameter,  $S_{11}$ , magnitude of the electric field intensity vector, and volumetric dissipated power loss density within the load, from the previous to the current mesh. Figure 7 depicts the magnitude of  $S_{11}$  within the operating frequency range of the WR975, electric field intensity vector within the waveguide and cavity, and volumetric power loss density within the load for cases involving an initial

mesh, a second mesh which is finer in spatial resolution by a factor of 1.5, and a third mesh which is finer by a factor of 2.

The parameters of the initial OGFDTD and OGF mesh [Al-Rizzo *et al.*, 2006] used to generate the results shown in Fig. 7 were chosen as  $\delta_r = \delta_z = 1.0156$  cm,  $\delta_\phi = 4.0^\circ$ ,  $n_{rin} = 12$ ,  $n_{rout} = 15$ . To ensure the stability of the EM algorithm,  $\delta_t$  is taken as  $1.8215 \times 10^{-11}$  s. The number of periods required for the EM fields to reach steady state is taken as 30. Results depicted in Fig. 7 show that the initial mesh is fine enough to ensure sufficient spatial resolution of the EM fields and temperature.

Next, a similar convergence test has been conducted to verify the accuracy of the OGF model using the same three meshing structures used to generate the results displayed in Fig. 7. The transient temperature profiles were calculated at the positions of the thermocouples for the three meshes. The OGF model for the initial mesh has been time stepped with an increment  $\delta_t' = 2.5$  s, which satisfies the stability constraint derived in [Al-Rizzo *et al.*, 2006]. It should be remarked that the majority of computational time in the CET model is consumed in updating the EM fields. Due to the axial symmetry of the cavity and excitation, the temperatures calculated on the four probes of “Bed Middle” as well as on the three probes of the “Bed Top” were identical. As seen in Fig. 8, numerical results provided by our CET model agree very well with those obtained from ePHYSICS. It should be noted, however, that the temperature dependency of  $\epsilon_r$  cannot be incorporated in the current versions of HFSS and ePHYSICS. We considered conduction and radiation heat transfer mechanisms in both the CET and ePHYSICS. In the CET model, the local temperature dependency of the EM constitutive parameters has been incorporated and the temperature inside the empty region of the cavity is considered to be temperature dependent and is updated in each computational cycle of the OGF thermal solver while the temperature in this region has been

**Figure 7.**  $S_{11}$  spectrum, magnitude of the electric field intensity vector (V/m) along the  $z$  axis, and volumetric dissipated power loss density within the load ( $W/m^3$ ) along the  $z$  axis for three different meshing schemes.



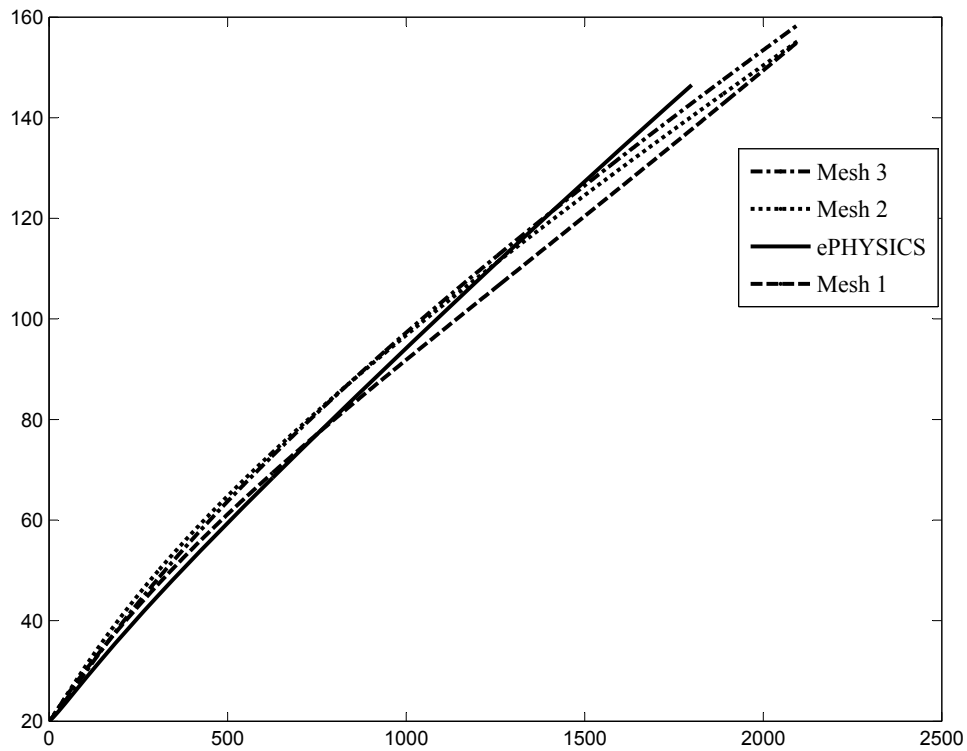
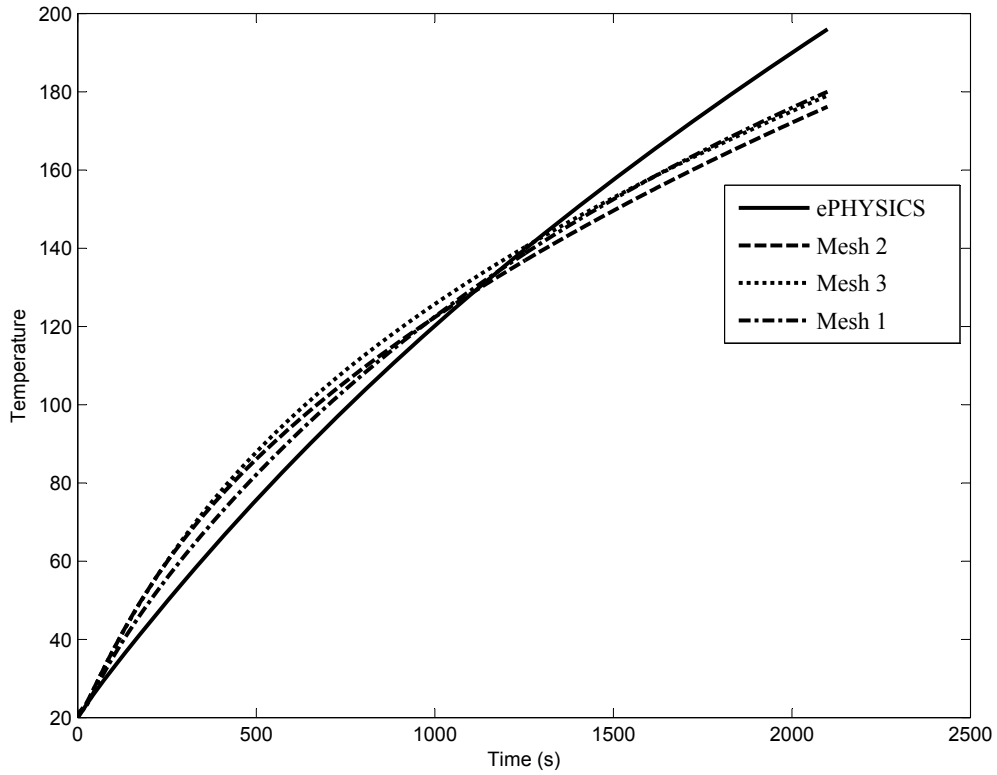
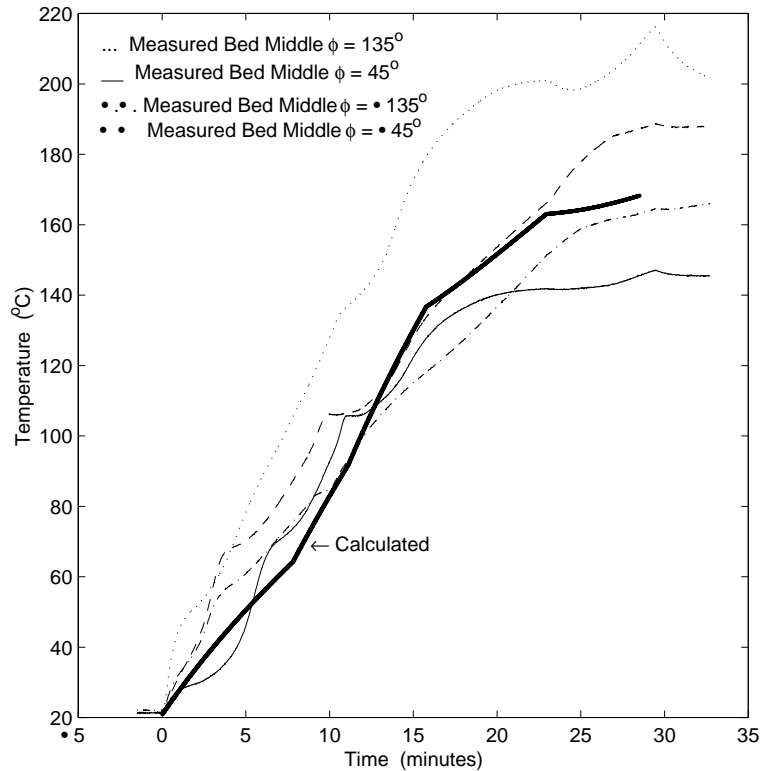


**Figure 8.** Temperature on the “Bed Middle” and “Bed Top” layers computed from the CET using three different meshing schemes and Ansoft’s ePHYSICS.

**Figure 9.** Comparison between measured and calculated temperatures on the “Bed Middle” layer at 909 MHz



considered constant throughout the exposure period in ePHYSICS and is fixed at 200 °C. A single, constant convective heat transfer coefficient,  $h=15$ , has been used in ePHYSICS while a value of 0.2 has been assumed for the emissivity of the radiation thermal boundary against a 20 °C reference ambient temperature for both the CET model and ePHYSICS.

Figure 9 presents the transient temperature profiles on the “Bed Middle” layer calculated at 909 MHz. The four thermocouples on the “Bed Middle” layer did not yield identical measured temperatures. For the convenience of comparison, an average of the temperatures measured by the four thermocouples is shown in Fig. 10. Figure 11 presents the computed temperature evolution on the “Bed Top” layer along with the measured temperatures. We have noticed more inconsistencies among the three measured temperatures on the “Bed Top” compared to those of the four measured temperatures on the “Bed Middle” layer. It should be noted that the calculated temperature in the “Bed Top” layer

matched well with one of the three measured temperatures. Since the measured temperatures on the “Bed Top” layer present larger inconsistencies with each other, the most remarkable differences between the calculated and average measured temperatures can be seen in Fig. 12, particularly in the late stage of heating.

In the above simulations, we used  $d\epsilon_r' = 0.1$ ,  $d\epsilon_r'' = 0.05$ . This means that when the average change of the real part of the complex relative dielectric constant,  $\epsilon_r'$  reaches 0.1 or the average change of the imaginary part,  $\epsilon_r''$  reaches 0.05, the EM fields are recalculated. For this case, the EM field calculations are executed five times, and the values of the amplitude of the reflection coefficient, which is the ratio of the amplitudes of the reflected to the incident electric field intensity vector at the input port of the feed waveguide,  $S_{11}$  calculated for each run, are listed in Table 1.

Next, calculations were performed at 915 MHz. Figure 13 (a), (b) compares the measured/average temperatures on the “Bed Middle” layer

**Figure 10.** Comparison between average measured and calculated temperatures on the “Bed Middle” layer at 909 MHz

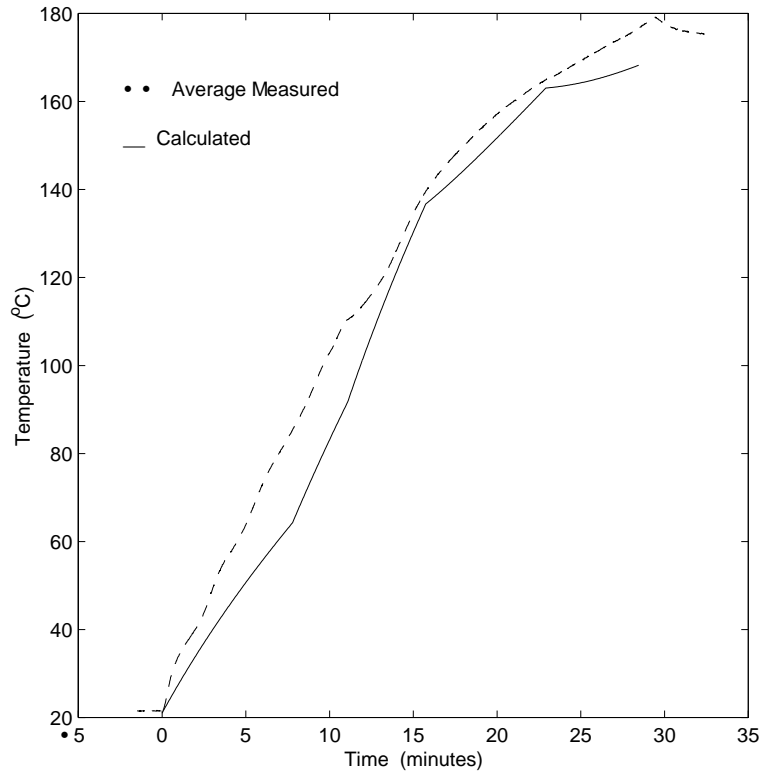


**Figure 11.** Comparison between measured and calculated temperatures on the “Bed Top” layer at 909 MHz

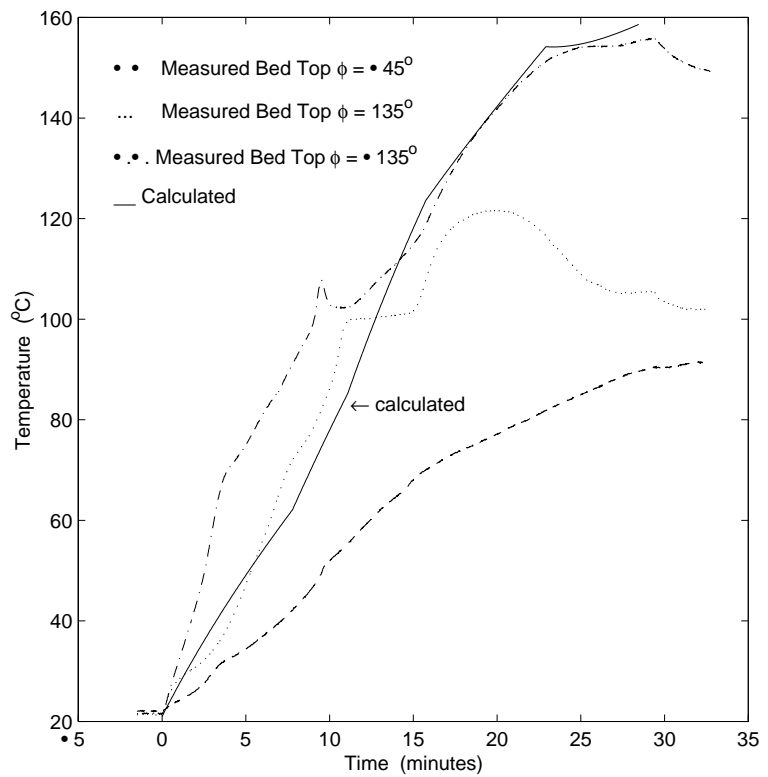
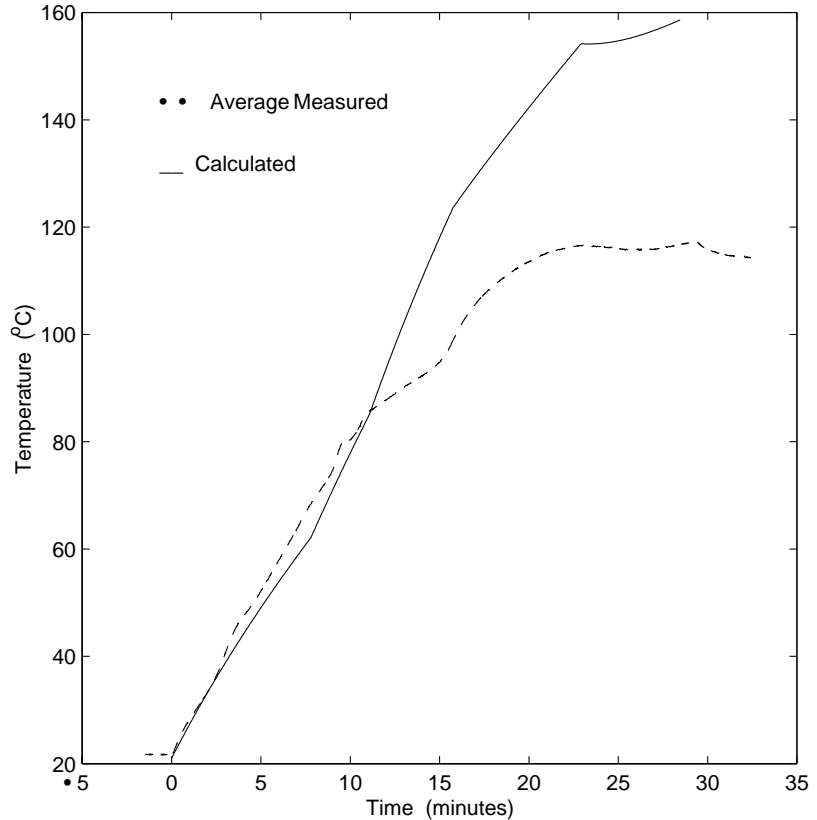


**Figure 12.** Comparison between average measured and calculated temperatures on the “Bed Top” layer at 909 MHz



against the calculated values at 909 MHz and 915 MHz. Figure 14 (a) (b) compares the measured/average temperatures on the “Bed Top” layer against the calculated values at 909 MHz and 915 MHz. Results shown in Figs. 13 and 14 clearly demonstrate the dependency of the computed temperatures on the central frequency of the magnetron.

The computational time and accuracy are largely determined by the parameters  $d\epsilon_r'$  and  $d\epsilon_r''$ . Choosing too small values of  $d\epsilon_r'$  and  $d\epsilon_r''$  will significantly prolong the computational time. Conversely, taking too large values may deleteriously affect the computational accu-

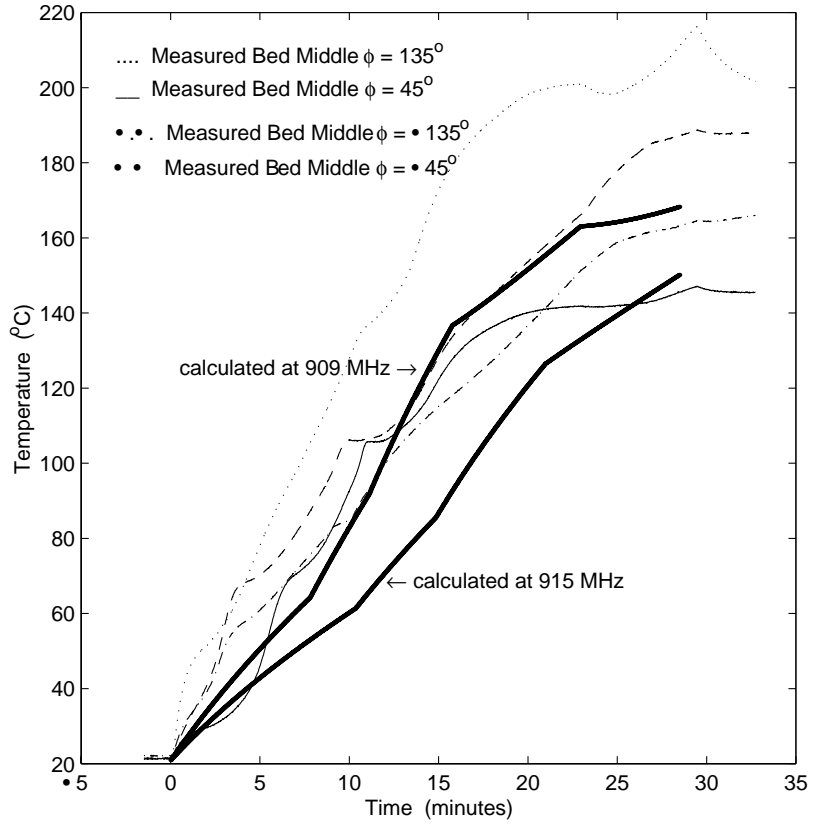
racy. Therefore, a compromise must be made in terms of the particular type of the processed material.

Figure 15 compares the temperature on the “Bed Middle” layer calculated at 909 MHz for  $d\epsilon_r' = 0.1$ ,  $d\epsilon_r'' = 0.05$  and  $d\epsilon_r' = 0.05$ ,  $d\epsilon_r'' = 0.02$  with the average measured temperature. Figure 16 compares the temperature on the “Bed Top” layer calculated at 909 MHz for  $d\epsilon_r' = 0.1$ ,  $d\epsilon_r'' = 0.05$  and  $d\epsilon_r' = 0.05$ ,  $d\epsilon_r'' = 0.02$  with the average measured temperature. From Figs.15 and 16, it is seen that changing the parameters from  $d\epsilon_r' = 0.1$ ,  $d\epsilon_r'' = 0.05$  to  $d\epsilon_r' = 0.05$ ,  $d\epsilon_r'' = 0.02$ , the corresponding computed

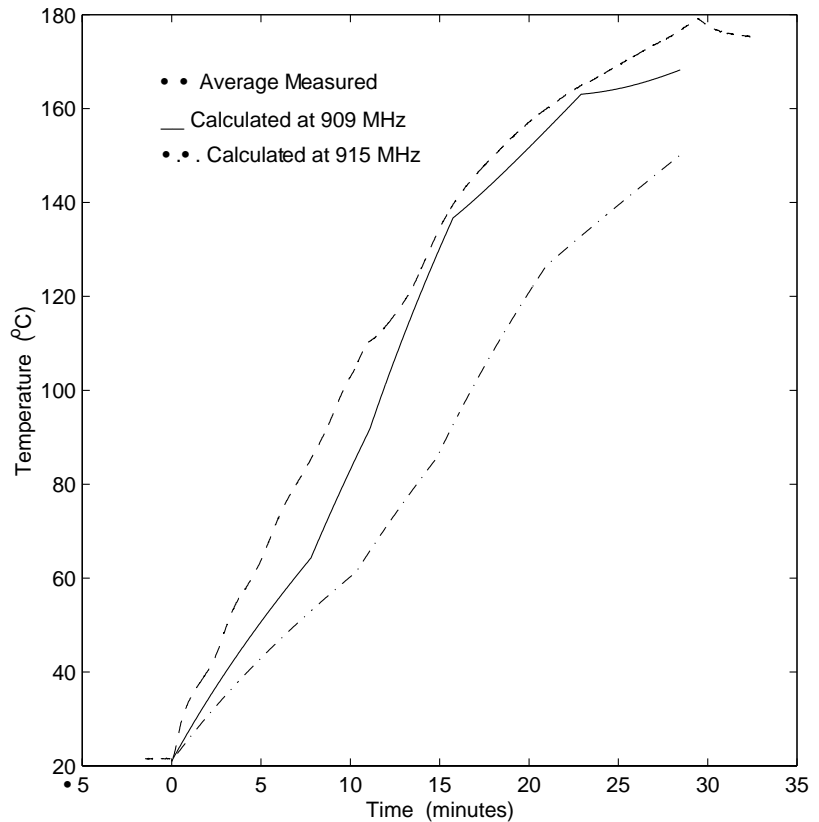
**Table 1.**  $S_{11}$  calculated at different instants during the heating of a mineral ore sample exposed to 12.5 kW, 909 MHz microwave energy with  $d\epsilon_r' = 0.1$ ,  $d\epsilon_r'' = 0.05$

Time (s)	0.0	467.5	665	945	1375
$ S_{11} $	0.774	0.781	0.781	0.778	0.780

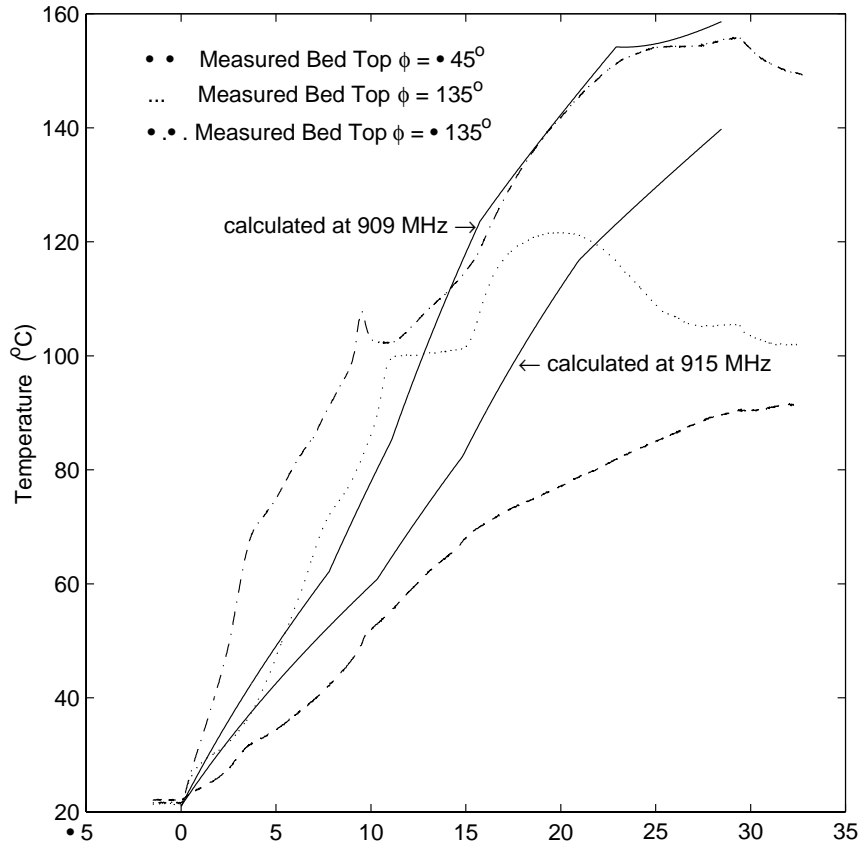
**Figure 13(a).** Comparison between measured and calculated temperatures on the “Bed Middle” layer at 915 MHz



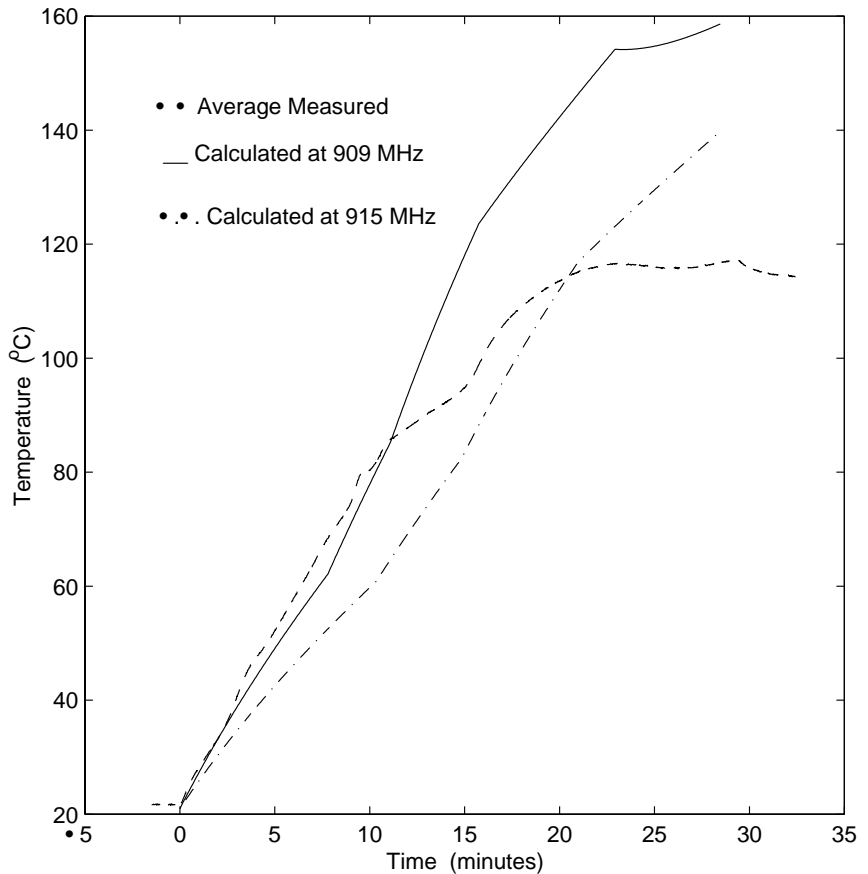
**Figure 13(b).** Comparison between average measured and calculated temperatures on the “Bed Middle” layer at 915 MHz



**Figure 14(a).** Comparison between measured and calculated temperatures on the “Bed Top” layer at 909 MHz and 915 MHz



**Figure 14(b).** Comparison between average measured and calculated temperatures on the “Bed Top” layer values at 915 MHz



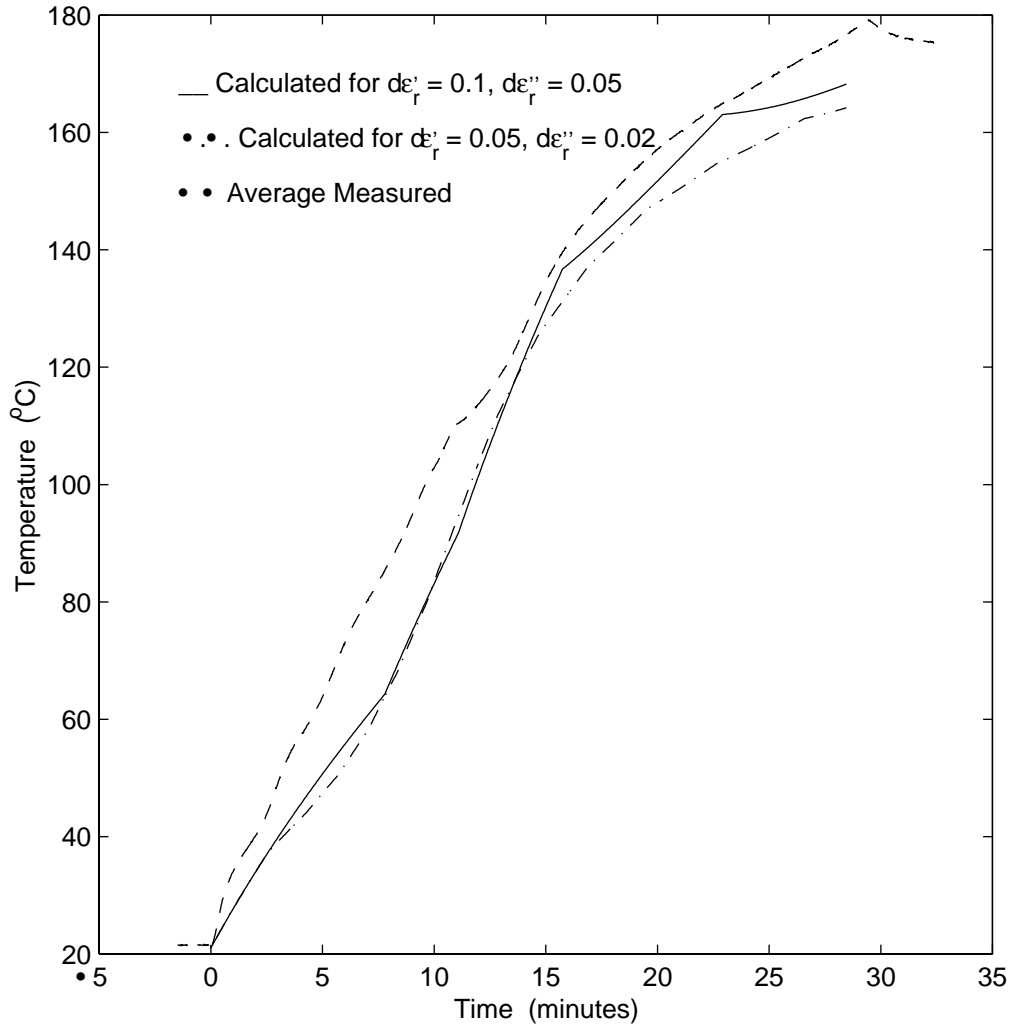


**Figure 15.** Comparison between average measured and calculated temperatures on the “Bed Middle” layer at 909 MHz for  $d\epsilon_r' = 0.1$ ,  $d\epsilon_r'' = 0.05$  and  $d\epsilon_r' = 0.05$ ,  $d\epsilon_r'' = 0.02$

temperatures did not change significantly though the temperature rise calculated for  $d\epsilon_r' = 0.05$ ,  $d\epsilon_r'' = 0.02$  is quite smooth. This is because the dielectric constant of the processed material does not change drastically over the temperature range of consideration.

For the case with  $d\epsilon_r' = 0.05$ ,  $d\epsilon_r'' = 0.02$ , 14 field calculations are performed. The computational time is significantly longer than that consumed when  $d\epsilon_r' = 0.1$ ,  $d\epsilon_r'' = 0.05$ . In Table 2 we present the values of  $S_{11}$  obtained in the 14 field calculations.

The above analysis and comparisons

demonstrate that the proposed CET model have successfully predicted the main features of the dynamic temperature distributions. As expected, there exist some discrepancies between the calculated and measured temperatures, and this may be attributed to a number of factors. These include uncertainties in the physical parameters used in the simulation, particularly those of the thermal model; material phase change; and energy released from exothermic chemical reactions observed at the late time of the curing process, which may have added to the volumetric heat generation term. On the other

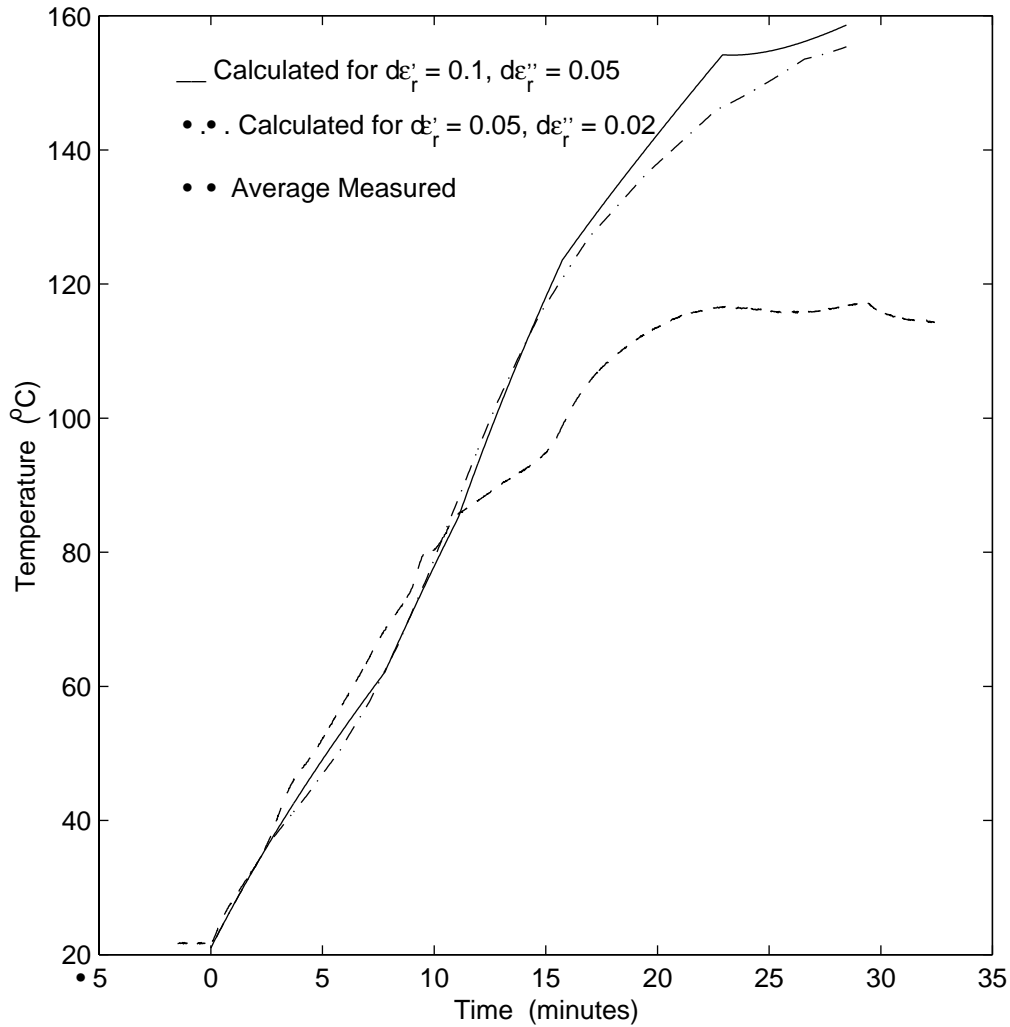


**Figure 16.** Comparison between average measured and calculated temperatures on the “Bed Top” layer at 909 MHz for  $d\epsilon_r' = 0.1$ ,  $d\epsilon_r'' = 0.05$  and  $d\epsilon_r' = 0.05$ ,  $d\epsilon_r'' = 0.02$

**Table 2.**  $S_{11}$  amplitudes calculated at different instants during the heating of a mineral ore sample exposed to 12.5 kW, 909 MHz microwave energy with  $d\epsilon_r' = 0.05$ ,  $d\epsilon_r'' = 0.02$

Time(s)	0	155	257.5	345	425	502.5	582.5
$ S_{11} $	0.774	0.783	0.790	0.789	0.787	0.785	0.784
Time(s)	670	770	882.5	1015	1170	1357.5	1595
$ S_{11} $	0.783	0.782	0.779	0.778	0.777	0.780	0.790

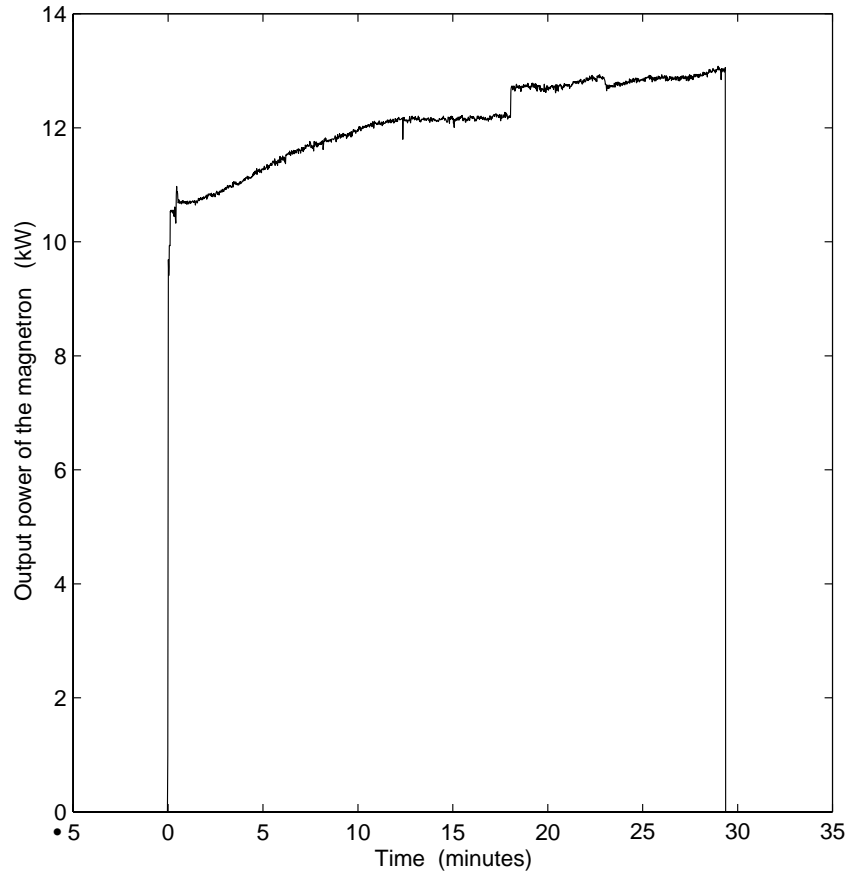


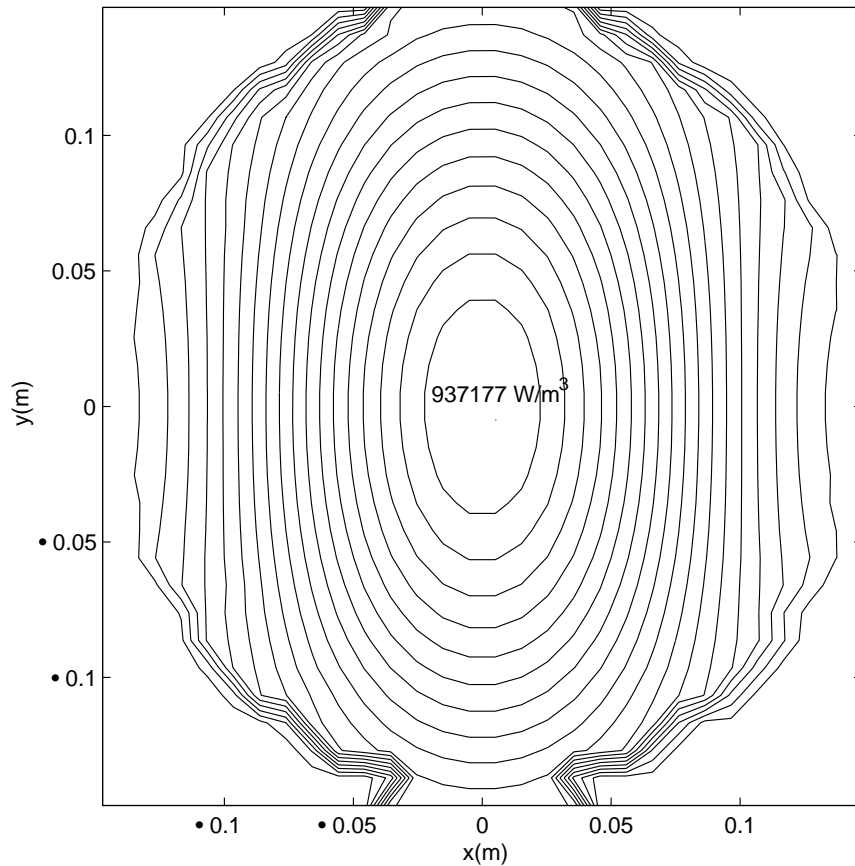
**Figure 17.** Output power of the magnetron during the heating process

hand, it is conceivable that a uniform loading and compaction of the material and minimization of air pockets could further improve the agreement between simulations and experimental measurements. Inhomogeneities experienced in sample loading were identified as the key likely cause for most of the discrepancies between temperatures measured by the different thermocouples on the two layers. The inevitable fluctuation of the frequency and output power of the magnetron is another important source. Small variations in the frequency and/or power coupled to the cavity may cause the induced temperature profiles to evolve in a different manner. An input power of 12.5 kW is used in the simulations, but actually, the output power of the magnetron in operation fluctuated between about 10 kW and 13 kW, as shown in Fig. 17.

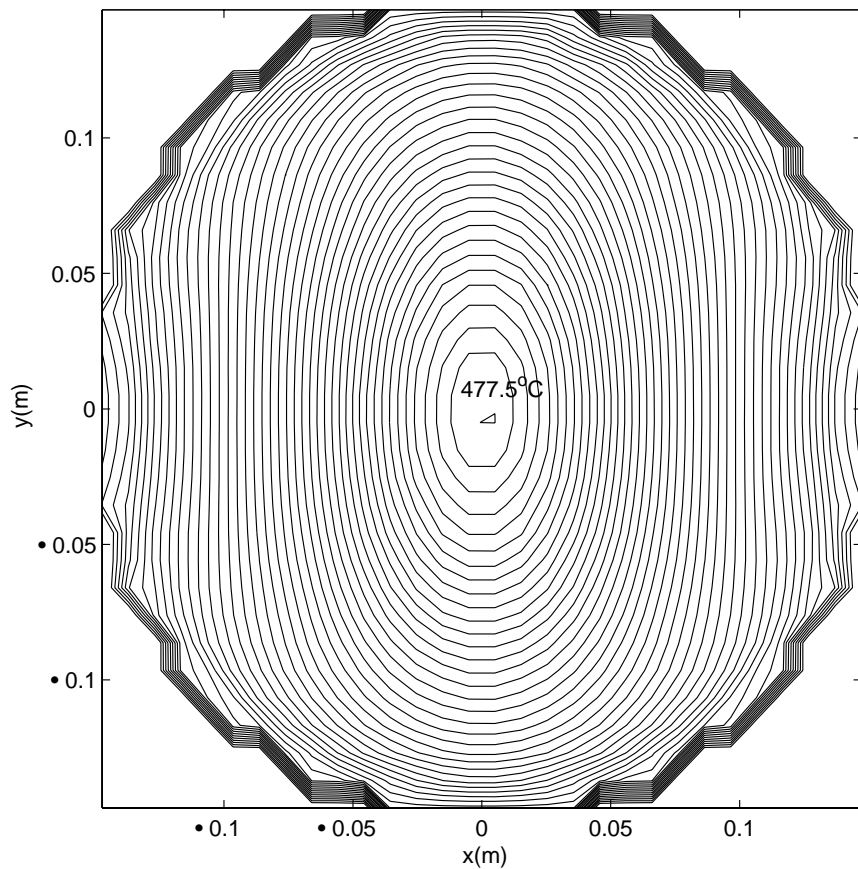
In the above, the temperature is provided only at points corresponding to the locations of the thermocouples. Simulations were also carried out to determine the temperature distributions in some geometrical cross-sections at the end of the heating process. As an example, Figs. 18(a) and (b) show the power density and temperature on an  $x$ - $y$  plane passing through the center of the load, 11.4 cm away from the inner bottom surface of the applicator. Similarly, Figs. 19(a) and (b) present the power density and temperature on an  $x$ - $y$  plane positioned along the interface between the load and air. Finally, Figs. 20(a) and (b) depict the power density and temperature on the plane  $x = 0$  within the processed material passing through the center of the load.

From these volumetric dissipated power and

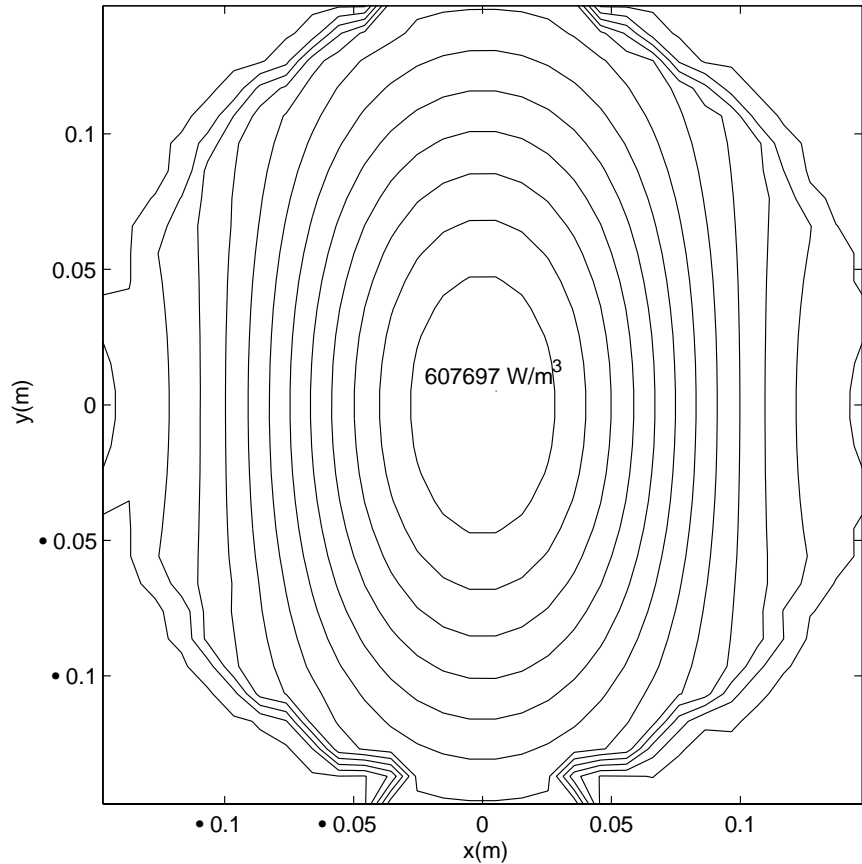
**Figure 18 (a).** Power density calculated on an  $x$ - $y$  plane located at the center of the workload, the contour level difference =  $50000 \text{ W/m}^3$



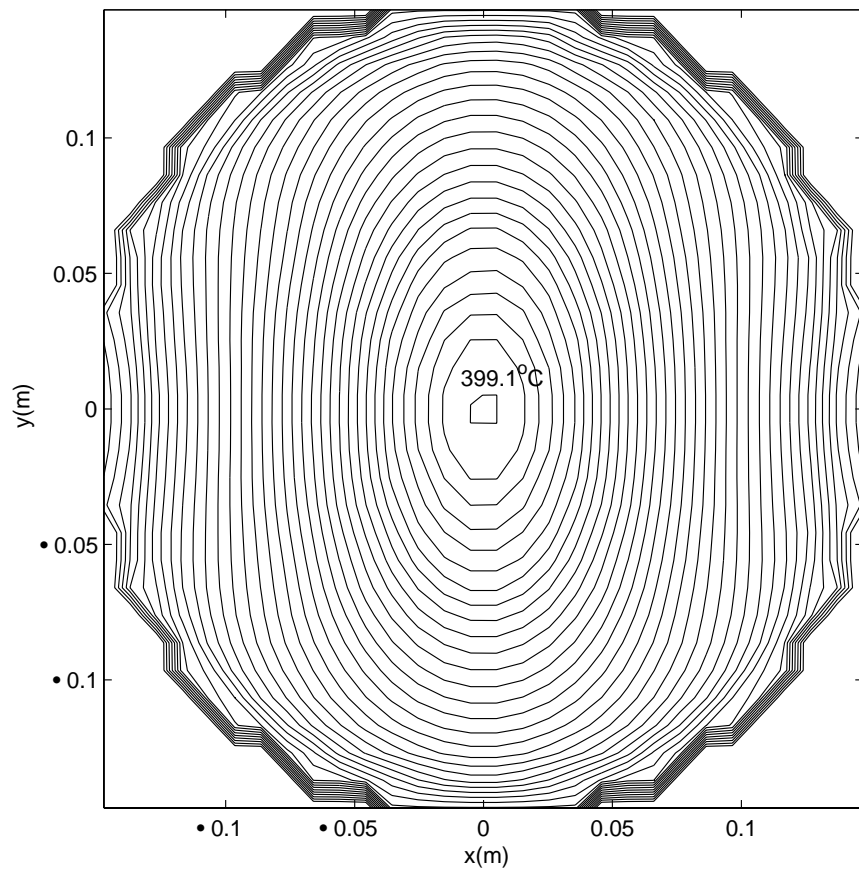
**Figure 18 (b).** Temperature distribution on an  $x$ - $y$  plane located at the center of the workload, the contour level difference =  $10^\circ \text{ C}$



**Figure 19 (a).** Power density calculated on the surface of the workload, the contour level difference =  $50000 \text{ W/m}^3$



**Figure 19 (b).** Temperature distribution on the surface of the workload, the contour level difference =  $10^\circ \text{ C}$



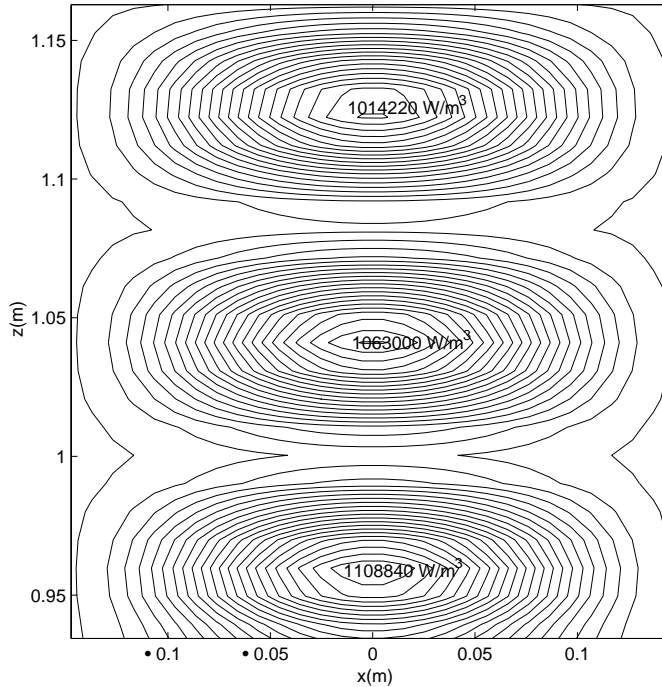


**Figure 20(a).** Power density calculated on the plane  $x = 0$  within the workload, the contour level difference =  $50000 \text{ W/m}^3$

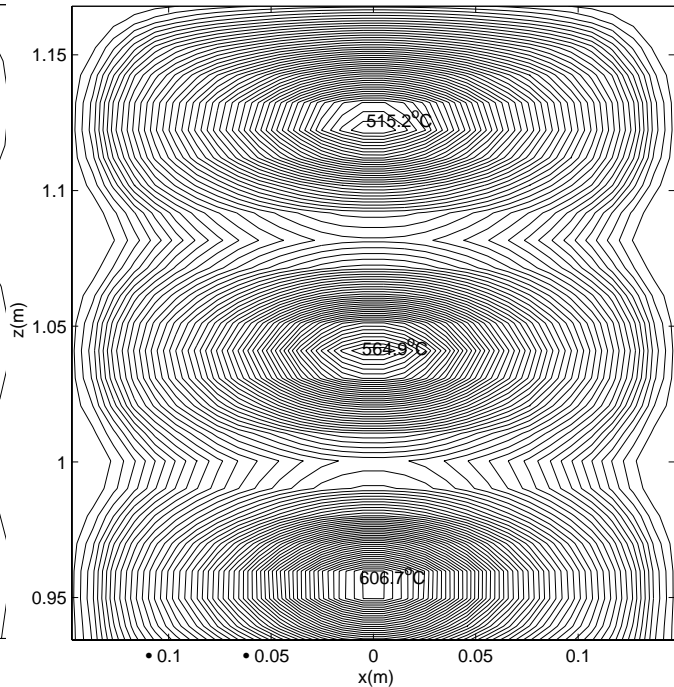


**Figure 20(b).** Temperature distribution on the plane  $x = 0$  within the workload, the contour level difference =  $10^\circ \text{ C}$

temperature distributions, some common features of the heating pattern can be observed. For example, most of the heating has occurred around the central region of the workload than elsewhere. We note that the power density and temperature distributions have similar patterns. This is because no significant heat transfer mechanisms have occurred during the irradiation process. At the end of the curing process, heat flow into air inside the applicator is only 1.53 W; heat flow through a cylindrical surface within the treated material with radii of 13.2 cm, 14.2 cm, and 15.0 cm are 127.8 W, 186.7 W, and 337.7 W, respectively; heat flow through an  $x$ - $y$  plane within the workload with a distance from the surface of the dielectric of 2.0 cm, 13.2 cm, and 21.3 cm are 2.3 W, 102.1 W, and 123.8 W, respectively. These values of heat flow are small compared with the power absorbed by the processed material, which at an input power of 12.5 kW and a frequency of 915 MHz is 3414.71 W.

## CONCLUSIONS

Using numerical and experimental results, we have examined a microwave heating process in a cylindrical multimode applicator taking into account the variation of the dielectric properties of the workload with change in temperature. Several examples are presented for the temporal and spatial evolution of the temperature. Temperature patterns measured at selected points within the processed material are compared against calculated values. The comparisons demonstrated that the simulations correctly predicted the main features of temperature evolution. Results obtained at 909 and 915 MHz showed that similar to the frequency selectivity of the EM characteristics of the resonant applicator, the heating patterns are also sensitive to very small changes in frequency. The discrepancies between measured and computed temperatures are attributed to uncertainties in the thermal properties of the

---

workload, inhomogeneous packing, fluctuations in the power and frequency of the magnetron, and release of heat due to exothermic chemical reactions.

## REFERENCES

- Al-Rizzo, H. M., J. M. Tranquilla, and Ma Feng (2005). "A finite difference thermal model of a cylindrical microwave heating applicator using locally conformal overlapping grids: Part I - Theoretical formulation," *J Microwave Power & Electromag. Energy* 40(1), pp. 17-29.
- Al-Rizzo, H. M., Ma Feng, and J. M. Tranquilla (2000). "Incorporation of waveguide feed and cavity wall losses in a Cartesian/cylindrical hybrid finite-difference time domain (FD-TD) analysis of microwave applicator," *J. Microwave Power & Electromag. Energy*, 35(2), pp. 110-118.
- Braunstein, J., K. Connor, S. Salon, and L. Libelo (1999). "Investigation of microwave heating with time varying material properties," *IEEE Trans. Magnetism* 35(3), pp. 1813-1816.
- Clemens, M., E. G. Jonaj, P. Pinder, and T. Weiland (2000). "Numerical simulation of coupled transient thermal and electromagnetic fields with the finite integration method," *IEEE Trans. Magnetism* 36(4), pp. 1448-1452.
- Dibben, D. C. (1995). *Numerical and experimental modeling of microwave heating applications*, Ph.D. Thesis, University of Cambridge, UK.
- Filfet, A. W., et al. (1996). "Application of microwave heating to ceramic processing: Design and initial operation of a 2.45-GHz single-mode furnace," *IEEE Trans. Plasma Sci.* 24(3), pp. 1041-1049.
- Gamos, J. P. (1998). *Analysis of aperture-coupled microwave cavity resonators using vector finite elements*, Ph.D. Thesis, University of Akron.
- Haala, J. and W. Wiesbeck (2002). "Modeling microwave and hybrid heating processes including heat radiation effects," *IEEE Trans. Microwave Theory Tech.*, 50(5), pp. 1346-1354.
- Iskander, M. F., et al. (1994). "FDTD simulation of microwave sintering of ceramics in multimode cavities," *IEEE Trans. Microwave Theory Tech.*, 42(5), pp. 793-800.
- Ma, L., et al. (1995). "Experimental validation of a combined electromagnetic and thermal FDTD model of a microwave heating process," *IEEE Trans. Microwave Theory Tech.*, 43(11), pp. 2565-2572.
- Materials Research Society (MRS) Proceedings on "Microwave Processing of Materials" vol. 269, 1992; vol. 347, 1994, and vol. 430, 1996.
- Torres, F., and B. Jecko (1997) "Complete FDTD analysis of microwave heating processes in frequency-dependent and temperature-dependent media," *IEEE Trans. Microwave Theory Tech.*, 45(1), pp. 108-117.
- Tranquilla, J. M., M. Feng, and H. M. Al-Rizzo (1999). "A Cartesian-cylindrical hybrid FD-TD analysis of composite microwave applicator structures," *J. Microwave Power & Electromag. Energy*, 34(2), pp. 97-105.